TECHNICAL ARTICLE

An investigation on the microstructure and defects in the mechanically milled Cu and Fe powders

M. Mojtahedi,[1,a] M. Goodarzi,[1] M. R. Aboutalebi,[1] and V. Soleimanian[2]
[1]School of Metallurgy and Materials Science, Iran University of Science and Technology, Tehran, Iran
[2]Department of Physics, Faculty of Science, Shahrekord University, Shahrekord, Iran

(Received 9 December 2013; accepted 11 July 2014)

The microstructural characteristics of mechanically milled (MM) iron (Fe) and copper (Cu) powders are investigated by means of various X-ray crystallography analysis methods. The conventional Williamson–Hall and Warren–Averbach methods are used besides the modified Williamson–Hall, the modified Warren–Averbach, and the Variance approaches, in proper cases. Afterward, the obtained crystallite size and dislocation density are used to calculate the stored energy in the nanostructured powders. For this aim, a new geometrical approach is developed which can consider three-dimensional crystallites and the thickness of boundaries between them. Moreover, the released energy during annealing of MM Cu and Fe powders is measured using differential scanning calorimetry. The results of line broadening analysis and geometrical modelling are combined to the calorimetry of a room temperature aged Cu powder. In this way, the thickness of grain boundary in the nanostructured Cu is calculated to be 1.6 nm. © *2014 International Centre for Diffraction Data.*
[doi:10.1017/S0885715614000761]

Key words: nanostructure, XRD analysis, geometrical model, grain boundary thickness, interface energy

I. INTRODUCTION

In past decades, mechanical alloying and milling were used for synthesis of various categories of nanostructured materials such as elemental powders, super saturated solutions, and amorphous compounds (Suryanarayana, 2004). The main structural change during mechanical milling of pure metals is increase of the lattice defects. The reduction of crystallite size because of the application of mechanical energy goes along with the increase of volume fraction of grain boundaries (GBs). As a matter of fact, a noteworthy proportion of atoms is located inside or in the vicinity of GBs, triple junctions, and dislocation cells.

The augmentation of research in the field of nanomaterials and nanostructured materials caused a need for proper characterization methods. The common method for structural characterization of the mechanically milled (MM) metals is X-ray crystallography (XRD) analysis. The sample preparation is simple and the obtained characteristics are average of the entire sample. These can be empirical advantages over the powerful technique of transmission electron microscopy (TEM) (Tian and Atzmon, 1999; Gubicza and Ungar, 2007). Therefore, several XRD analysis methods have been developed to calculate the crystallite size, microstrain, or dislocation density in different lattice structures.

Copper (Cu) and iron (Fe) are among the most applicable engineering metals. Characteristics of nanostructural Cu and Fe powders are widely studied. However, dissimilar results are reported for MM powders. It is well established that the milling condition can affect the results, while the XRD analysis method should be considered as another possible reason of discrepancy. Some calculated crystallite sizes of the powders which were all produced by planetary ball mill are exhibited in Table I. It should be mentioned that despite the same milling apparatus, the milling energy can still be different. Nevertheless, a fraction of the observable disagreement of the literature data can be related to application of different diffraction analysis methods.

On the other hand, the expansion of GB network and structural defects results in storage of a valuable amount of energy in MM metals and alloys. There have been attempts to calculate the stored energy using a combination of the results of XRD analysis and diffraction scanning calorimetry (DSC) (Zhao *et al.*, 2001; Zhao *et al.*, 2002). However, in the majority of efforts GBs were assumed as two-dimensional (2D) planes. In recent works on the analysis of the mechanically alloyed Cu alloys, a spherical (Sheibani *et al.*, 2010; Mula *et al.*, 2012) or cubic (Aguilar *et al.*, 2009) shape was assumed for nanocrystallites. Therefore, the thickness and volume of boundaries were neglected, while in the case of nanostructured materials the interface volume and the proportion of triple junctions are notable parameters.

Efforts also have been made to consider the effect of boundary thickness on the interface volume fraction. A simple equation for estimation of the volume fraction of the boundaries is $3\delta/D$, proposed by Mütschele and Kirchheim (1987) in which δ stands for the boundary thickness and D is the grain size. Later, Palumbo *et al.* (1990) proposed that the intercrystalline fraction is equal to $1-[(D-\delta)/D]^3$. However, the effect of crystallites shape on the boundary volume still cannot be considered.

[a]Author to whom correspondence should be addressed. Electronic mail: mojtahedi@iust.ac.ir

TABLE I. The reported crystallite sizes of Cu and Fe powders, which are calculated by various XRD analysis methods. The samples are all produced by planetary ball-mill.

Material	Analysis method	Milling time (h)	Crystallite size (nm)	Reference
Copper	Scherrer–Wilson	10	18	Khitouni *et al.* (2009)
	Scherrer–Wilson	100	10.9	Zhao *et al.* (2002)
	WPPM	48	29	Fais and Scardi (2008)
	WPPM	24	35	Boytsov *et al.* (2007)
Iron	Scherrer	1	17	Le Brun, Gaffet *et al.* (1992)
	Scherrer	54	12.7	Guittoum *et al.* (2010)
	Scherrer–Wilson	140	7.6	Zhao *et al.* (2001)
	Williamson–Hall	45	19.2	Delshad Chermahini *et al.* (2009)

The aim of the present study is firstly to apply suitable XRD analysis methods for evaluating the microstructural characteristics of nanostructured Cu and Fe powders and secondly, to estimate the energy and thickness of crystallite interfaces in a three-dimensional (3D) approach. For this aim, a new geometrical model is derived for prediction of the volume fraction of interface and triple junctions in the nanostructured materials. Finally, the obtained results were combined with DSC experiments to estimate the average thickness of crystallite boundary in the nanostructural powders.

II. EXPERIMENTAL

A. Sample preparation

The nanostructured Cu and Fe powders were prepared using a planetary ball mill with hardened steel vials and balls. Each vial contained balls with diameters of 10 and 8 ml and were filled with argon gas before milling. The 99.8% purity Cu and Fe powders were subjected to 48 h of milling with the ball to powder weight ratio of 20:1 and the rotation speed of 370 RPM. Additionally, 1 wt% of Stearic acid was added to the powder mixture as lubricant. The samples are marked as Cu48 and Fe48. Finally, the contamination of Fe in the Cu powder because of milling apparatus was measured using wet chemical analysis, which was 0.4 wt%.

B. Characterization

The size and morphology of the milled powders were determined using scanning electron microscopy with secondary electron imaging. Afterward, XRD experiments were conducted at room temperature, using a PANalytical-Xpert diffractometer. Since the fluorescence of Fe powder under Cu$K\alpha$ radiation has a detrimental effect on the quality of XRD profiles, the experiments were conducted using Co$K\alpha$ radiation (1.78901 Å). The 2θ step was set at 0.02° and the counting time per step was 4 s, in the range of $2\theta = 40$–120°. In addition to the newly milled metals, a milled Cu sample which had aged at room temperature for 9 months was also subjected to the XRD analysis (marked as sample Cu48-9).

To calculate the instrumental broadening, the Caglioti equation (Caglioti *et al.*, 1958) was used:

$$\mathrm{FWHM}^2 = U\tan^2(\theta) + V\tan(\theta) + W \qquad (1)$$

FWHM is full width at half maximum of height of the peaks and U, V, and W are the indices which can be determined by the aid of a standard specimen. An annealed pure alumina sample was prepared as the standard sample. Afterward, the instrumental broadening and background were removed from the diffraction profiles using the software MarqX (Dong and Scardi, 2000), in which the background is calculated by a third-order polynomial function and the reflections are fitted using a pseudo-Voigt function. The refinement procedure is continued until a good agreement between the calculated and measured profiles is achieved. Afterward, determination of crystallite size and dislocation density was performed using the Williamson–Hall (WH) (Williamson and Hall, 1953), Warren–Averbach (WA) (Warren and Averbach, 1950), modified Williamson–Hall (MWH), modified Warren–Averbach (MWA) (Ungar and Borbely, 1996), and Variance (Wilson, 1962; Mitra and Mukherjee, 1981) methods. Finally, thermal analysis of the milled powders was performed in a Metler Toledo scanning calorimeter (DSC1); with a slow heating rate of 5 K min^{-1}, up to 700°C. About 10 mg of powder was used for each run.

III. RESULTS

A. Particle size

The overall morphology of Cu and Fe powders after 48 h of milling are shown in Figures 1(a) and 1(b), respectively. The Cu powder contains flaky particles with generally uniform size, whereas the Fe particles are rather equiaxed and agglomerated. On the other hand, the diameter of the milled Cu flakes is mostly in the range of 15–30 μm; while the Fe particles show size deviation in the range of 1–10 μm. As can be seen in Figures 1(c) and 1(d), both the Cu and Fe particles are formed by cold welding of smaller particles. It is also well known that severe plastic deformation of metals results in the formation of subgrain boundaries. Therefore, each powder particle contains several cold-welded grains and each grain may contain thousands of crystallites. Therefore, since the particle size of both powders is in the micrometer scale, they should be considered as nanostructured materials not nanomaterials.

B. XRD analysis: crystallite size and dislocation density

The XRD profiles of the samples are presented in Figure 2. According to the WH method, the volume-averaged crystallite size $\langle D_V \rangle$ and lattice microstrain $\langle \varepsilon^2 \rangle^{1/2}$ are related via Eq. (2).

$$\beta^* = \frac{1}{\langle D_V \rangle} + 2\langle \varepsilon^2 \rangle^{1/2} d^* \qquad (2)$$

In which β^* is the integral breath in the reciprocal space and d^* is the reciprocal lattice vector. The variation of β^*versus d^* for

https://doi.org/10.1017/S0885715614000761 Published online by Cambridge University Press

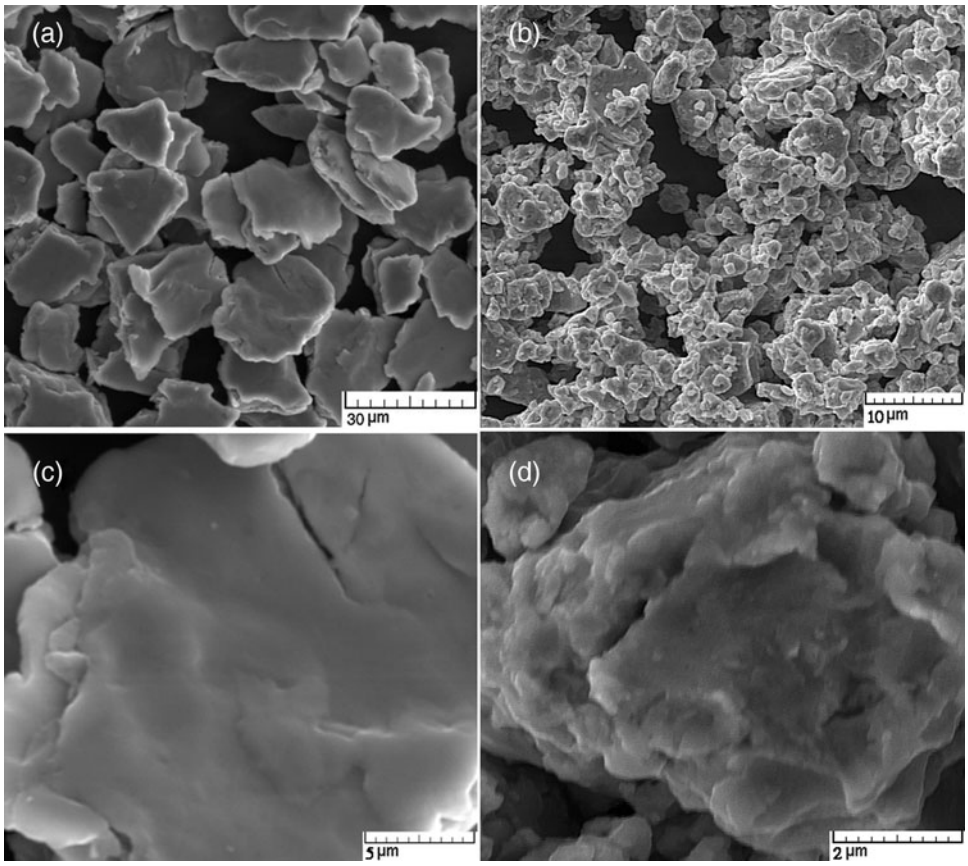

Figure 1. Secondary electron images showing: (a) morphology of Cu powder after 48 h of milling, (b) morphology of Fe powder after 48 h of milling, (c) typical shape of a single Cu particle, and (d) typical shape of a single Fe particle.

the sample Cu48 is plotted in Figure 3(a) and the resulted size and strain can be seen in Table II. However, the five data points do not have a linear trend and the parameter R^2 is just 0.54 for the fitted line. This can be caused by the effect of dislocations as a source of anisotropic strain broadening.

On the other hand, the crystallite size which results from the Scherrer equation (Langford and Wilson, 1978) in the <111> direction is near twice of the <311> direction. This may be interpreted as a sign of anisotropic size broadening. On the other hand, the strain anisotropy because of the formation of stacking faults in the (111) plane of face centered cubic (FCC) materials can affect the calculated crystallite size in the <111> direction. We have also calculated the crystallite size of Cu crystallites using Rietveld refinement (Mojtahedi *et al.*, 2013), which were 13.5, 7.6, 9.5, and 9.6 nm for (111), (200), (220), and (311) diffractions, respectively. It should be mentioned that the crystallite size in the <200>, <220>, and <311> directions are not significantly different. Therefore, the difference of calculated size in the <111> direction can be caused by a combination of crystallite shape and stacking faults.

A very common method for the estimation of the dislocation density in materials science is the equation of Williamson and Smallman (WS) (Williamson and Smallman, 1956):

$$\rho = \frac{2\sqrt{3}\langle \varepsilon^2 \rangle^{1/2}}{Db} \qquad (3)$$

where b and ρ are the Burgers vector length and the dislocation density, respectively. The effect of dislocations is also considered in the modified WH method, in which Eq. (2) is adjusted to the form of Eq. (4), where A is a factor related to the outer cut-off radius of dislocations (Re) and $\overline{C}_{hkl}$ is the average dislocation contrast factor.

$$\beta^* = \frac{0.9}{\langle D_V \rangle} + \left(\frac{\pi A^2 b^2}{2}\right)^{1/2} \rho^{1/2} d^* \overline{C}_{hkl}{}^{1/2} + O(d^* \overline{C}_{hkl}) \qquad (4)$$

The crystallite size can be calculated by plotting β^* versus $d^* \overline{C}_{hkl}{}^{1/2}$ and fitting a second-order equation. For this aim, the contrast factors of the edge and screw dislocations of Cu were calculated using the program ANIZC (Borbely *et al.*, 2003) (Table III). As can be seen in Figures 3(b) and 3(c), in the case of edge dislocations the variation of β^* versus $d^* \overline{C}_{hkl}$ is irregular and the fitting quality is poor, whereas in the case of screw dislocations a second-order polynomial equation can be well fitted to the data points. This indicates that the screw dislocation type has the main fraction among dislocations in the milled Cu powder. Finally, the crystallite sizes for samples Cu48 and Cu48-9 were calculated using the intercept of the corresponding curves (Table II).

The microstrain or the density of dislocations cannot be calculated via the MWH method. According to the WA method, the intensity of the diffraction peaks can be expressed via Eq. (5), in which $A(L)$ and $B(L)$ are the Fourier coefficients and

https://doi.org/10.1017/S0885715614000761 Published online by Cambridge University Press

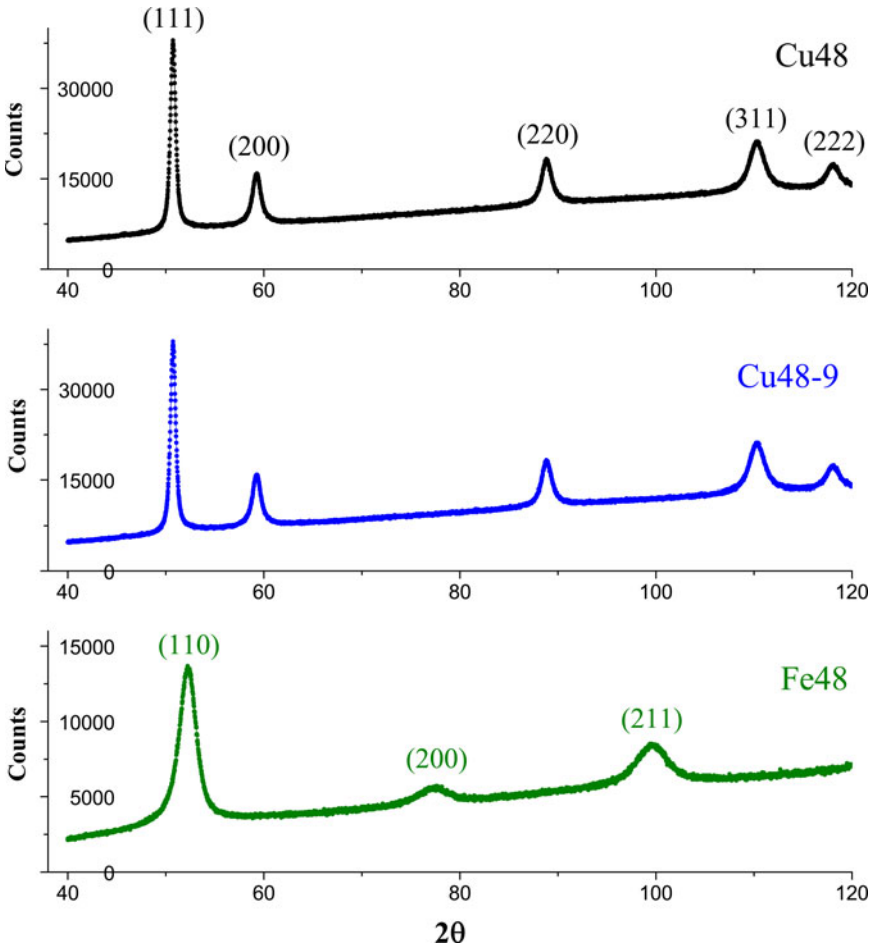

Figure 2. (Color online) The XRD profiles of Cu and Fe samples.

L is the Fourier length.

$$I(s) = K(s) \times \sum_{L=-\infty}^{L=+\infty} A(L)\cos\cos(2\pi Ls) + B(L)\sin\sin(2\pi Ls) \quad (5)$$

On the other hand, the microstrain, the diffraction vector and the Fourier coefficient of crystallite size $[A^S(L)]$, are related to each other via Eq. (6).

$$lnA(L) = lnA^S(L) + 2\pi^2 d_{hkl}^{*\,2}, L^2 < \varepsilon^2(L) > \quad (6)$$

On the basis of the works of Krivoglaz (Krivoglaz and Ryaboshapka, 1963; Krivoglaz, 1996) and Wilkens (Wilkens, 1976), it is stated that in the case of anisotropic broadening, Eq. (6) should be modified to the following form (Ungar and Borbely, 1996):

$$\ln A(L) = \ln A^S(L) - 1/2\rho b^2 L^2 \pi \ln\left(R_e/L\right) d^* 2\overline{C}_{hkl} + O(d^*)^4(\overline{C}_{hkl})^2 \quad (7)$$

Now the dislocation density can be calculated by plotting the variations of $\ln A(\ L\ )$ versus $d^{*\,2}\overline{C}_{hkl}$ for various quantities of L. The variations are plotted for the edge and screw dislocation types in Figures 4(a) and 4(b), respectively. Again the data for screw dislocations can be well fitted to a second-order equations; therefore the MWA method confirms the result of the MWH method about the principal dislocation type in the MM Cu powder.

The MWA method can be applied as a method for calculation of the dislocation density, which is more reliable than Eq. (3). For each of the assumed amounts of L in Figure 4(b), an equation in the form of $A(L)x^2 + B(L)x + C = 0$ can be resulted. Afterward, by plotting the variations of the term $B(L)/(\pi b^2 L^2/2)$ versus L, the dislocation density can be calculated.

The results of the WH, MWH, WA, and MWA methods for the milled Cu powders are collected in Table II. It can be seen that the WA method resulted in smaller crystallite size and higher microstrain than the WH method. As can be seen in Table II, deviation of results in the conventional WH method is too high. As previously mentioned, this inaccuracy is attributable to the application of linear fitting. The mathematical deviation becomes essentially smaller by application of the Modified form of WH plot.

The density of dislocations is calculated using the WS equation, as well as the MWA method. For this aim, the crystallite size and microstrain of Cu powders which are calculated from both of the WA and WH methods are inserted in Eq. (3). The estimated amounts of dislocation density are highly correlated to the XRD analysis method. It seems that more research is required to evaluate the precision of the results of various analysis methods for non-equilibrium nanostructured materials.

The obtained microstructural characteristics of the MM Fe powder by means of the WH and WA methods are also

https://doi.org/10.1017/S0885715614000761 Published online by Cambridge University Press

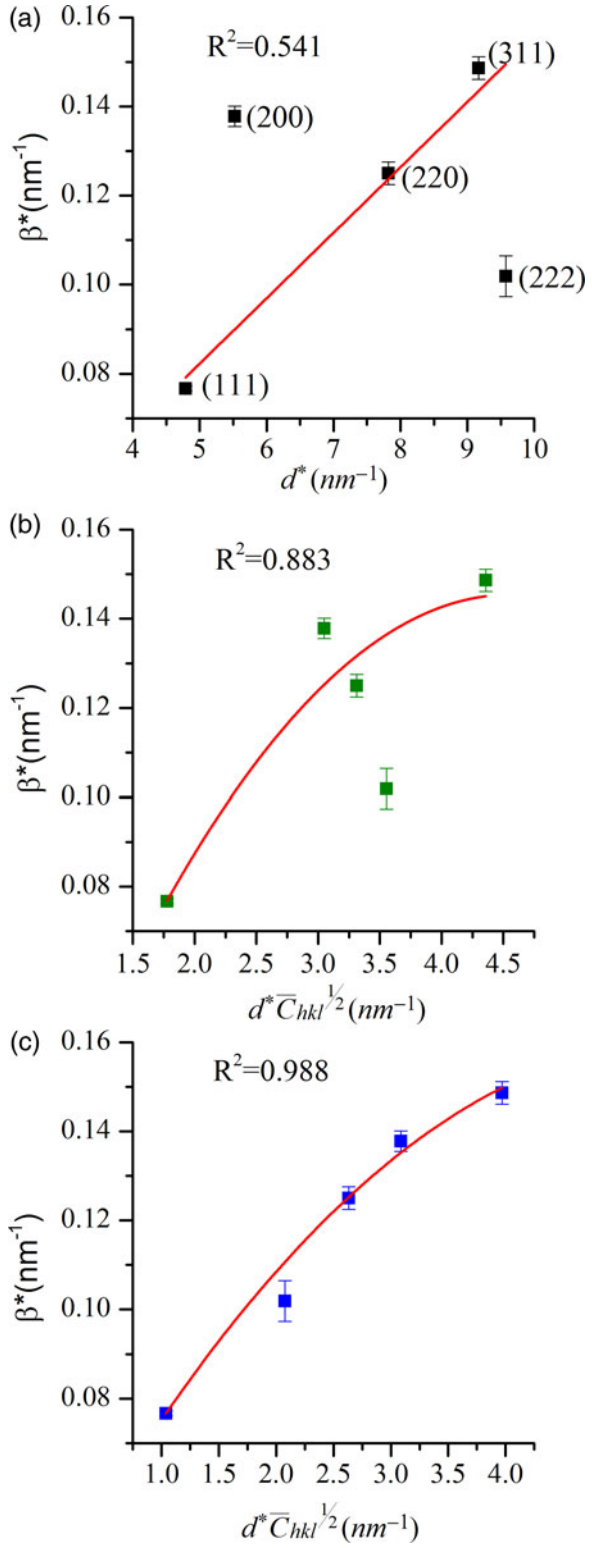

Figure 3. (Color online) The plots for the reflections of sample Cu48. (a) The WH plot. (b) The modified WH plot for edge dislocation type. (c) The modified WH plot for screw dislocation type.

imbedded in Table II. There were just three reflections of (110), (200), and (211) available in the diffraction range; therefore the calculated results may not be precise enough. Consequently, to obtain the crystallite size and dislocation density of Fe, the momentum method is applied despite the MWH and MWA methods. This method can provide adequate accuracy in the case of insufficient reflections. According to the works of Wilson (Wilson, 1962) and Groma (Groma, 1998), the *k*th-order moment of the intensity distribution $I(q)$ can be defined as:

$$M_k(q) = \int_{-q}^{q} q^k I(q)dq \Big/ \int_{-\infty}^{\infty} I(q)dq \tag{8}$$

In which $q = 2/\lambda(\sin\theta - \sin\theta_0)$, where θ_0 is the Brags angle. The different order moments and the Fourier transform of the intensity distribution are in the following relation:

$$M_k(q) = (i)^k \frac{1}{A(0)} \frac{d^k}{dL^k} A(L)|_{L=0} \tag{9}$$

Groma has calculated the second- and fourth-order moments as Eqs (10) and (11), respectively, in which ϵ_F is the crystallite size and $\Lambda = \pi/2g^2b^2\overline{C}$ (Borbély and Ungar, 2012), where g is the diffraction vector. The amounts of $\overline{C}$ and Λ for the diffraction peaks of Fe are expressed in Table IV. It should be noted that the dislocation character is unknown; therefore the dislocations are assumed to be half-edge and half-screw (Ungar *et al.*, 1998a, 1998b). Borbely and Groma (2001) have indicated that if the crystallite size causes notable broadening, the dislocation density could not be calculated from $M_2(q)$. In fact, evaluation of the dislocation density from $M_4(q)$ is more accurate.

$$M_2(q) = \frac{1}{\pi^2\epsilon_F} q - \frac{L}{4\pi^2 K^2 \epsilon_F^2} + \frac{\Lambda\langle\rho\rangle \ln(q/q_0)}{2\pi^2} \tag{10}$$

$$\frac{M_4(q)}{q^2} = \frac{1}{3\pi^2\varepsilon_F} q + \frac{\Lambda\langle\rho\rangle}{4\pi^2} + \frac{3\Lambda^2\langle\rho^2\rangle}{4\pi^2 q^2} \ln^2(q/q_1) \tag{11}$$

To utilize the Variance method, a pseudo-Voight function was fitted to each reflection profile. In this way, the FWHM and the fraction of Lorentzian function were obtained for each peak and then the fourth moment of each reflection was calculated. The variations of $M_4(q)/q^2$ versus q are plotted in Figure 5. Finally, a linear function is fitted to the first linear zone of each curve and ϵ_F is calculated from the slope of the lines. On the other hand, to calculate the dislocation density, $\overline{C}_{hkl}$ is calculated for each of the reflections of Fe. Afterward, the parameter of Λ is determined and $\Lambda\ \langle\ \rho\ \rangle$ is plotted versus Λ. The dislocation density is then calculated by a linear fit. As can be seen in Table II, the dislocation densities of Fe which are calculated using the WS method are too high, while the result of the Variance method is in a reasonable range.

III. DISCUSSION

A. Geometrical modelling of a nanostructured material

The truncated octahedral (TO) is widely applied as a representative of the 3D geometry of grains and cellular structures (Aste *et al.*, 1996; Pari and Misiolek, 2008). In this study, we also considered the boundaries between TO grains as 3D spaces. Schematic illustration of the crystallites and the related interface volumes are shown in Figures 6(a) and 6(b), respectively. The 2D or 3D hexagonal shapes are also used for modelling the microstructural behaviour of nanostructured

https://doi.org/10.1017/S0885715614000761 Published online by Cambridge University Press

TABLE II. The crystallite size, microstrain, and dislocation density of ball-milled Cu and Fe powders, calculated using different XRD analysis methods.

Sample	Size (nm)	Microstrain (%)	Method	ρ ($\times 10^{15}$ m^{-2})	Method
	20.9 ± 13.4	0.15*	WH	1.00*	WS
Cu48	12.9 ± 0.0	0.40 ± 0.01	WA	4.17 ± 0.65	WS
	26.6 ± 5.28	–	MWH	2.08 ± 0.23	MWA
	21.8 ± 13.4	0.15*	WH	0.97*	WS
Cu48-9	13.0 ± 0.1	0.39 ± 0.01	WA	4.05 ± 0.63	WS
	26.7 ± 7.19	–	MWH	2.06 ± 0.31	MWA
	10.1*	0.92 ± 0.87	WH	12.71*	WS
Fe48	2.6 ± 0.1	0.63 ± 0.03	WA	36.66 ± 7.44	WS
	3.9 ± 0.87	–	Variance	6.97 ± 0.58	Variance

*The calculated deviation was higher than the data itself.

materials (Yamakov *et al.*, 2002; Shimokawa *et al.*, 2005). Here, 3D prisms with hexagonal base are applied, which are presented in Figure 7(a). As can be seen in Figure 7(b), the thickness of GB boundary is presented by m. Flaky and columnar crystallites will be modelled by changing the ratio of dimensions of the prism.

In the next step, it is necessary to assume a reasonable amount for the interface thickness. It is common to assume $m = 0.5$ nm, while the inter-crystalline disordered regions may be wider in the deformed materials. Some available data about GB width of elemental metals can be seen in Table V. It can be seen that the diffusional width is normally about 0.5 nm, while the reported structural widths show more variations. The presence of a layer with internal stress around GBs (Guo *et al.*, 2013) can be the source of this variation. The relaxation of boundaries under low-temperature annealing of Fe powder is proved by HRTEM imaging (Jang and Atzmon, 2006). It is also shown that far from equilibrium interfaces can have various thicknesses (Li *et al.*, 2000). However, it would be possible to consider a larger average boundary width in the deformed nanostructured metals. Therefore, the boundary width of the MM metals is stated as a variable in the following calculations.

1. Truncated octahedral

The volume of a TO in Figure 6(a), with the edge length of s, is equal to:

$$V_{\mathrm{TO}} = 8\sqrt{2}s^3 \tag{12}$$

As is displayed in Figure 6(b), four kinds of space exist around each TO: the spaces between two square sides (six pieces), the spaces between two hexagonal sides (eight pieces), the spaces between three edges (36 pieces) which can be representative of triple junctions, and the spaces between four corners (24 pieces), which can illustrate the vortex points. To calculate the interface volume which belongs to each crystallite, the volume of each of the mentioned spaces should be multiplied to its total number around a single TO, and then to the fraction of that space which is related to each crystallite. Therefore, the relation of interface volume for each TO crystallite and the interface thickness is:

$$V_{\mathrm{TO}}^{IS} = 2\sqrt{3}\,s^2\,m + 6\sqrt{3}\,s^2\,m + 3.266\sqrt{3}\,m^2\,s + \sqrt{3}/2m^3 \tag{13}$$

The number of crystallites in one mole of milled materials can be calculated via Eq. (14), in which V^{m} is the molar volume.

$$n_{\mathrm{TO}} = \frac{V^m}{8\sqrt{2}(s + \frac{m}{\sqrt{6}})^3} \tag{14}$$

Finally, the total volume of interface in one mole of material can be calculated:

$$V_{\mathrm{TO}}^{I} = (n_{\mathrm{TO}}) \times \left(2\sqrt{3}\,s^2\,m + 6\sqrt{3}\,s^2\,m + 3.266\sqrt{3}\,m^2\,s + \sqrt{3}/2m^3\right) \tag{15}$$

TABLE III. Contrast factors of the edge and screw dislocations for the diffraction planes of Cu.

Diffraction plane	$\overline{C}_{\mathrm{edge}}$	$\overline{C}_{\mathrm{screw}}$
111	0.1378	0.0470
200	0.3048	0.3124
220	0.1795	0.1133
311	0.2261	0.1874
222	0.1378	0.0470

2. Hexagonal prism

As can be seen in Figure 7(a) the geometry of a prism with hexagonal base can be defined by three dimensions of L_1, L_2, and L_3. There are seven shapes of space at the interfaces of each crystallite, which are shown in Figure 7(b). Calculation of the volume of these interfacial spaces using three dimensions of L_1, L_2, and L_3 is difficult; therefore additional dimensions are define in Figure 7(c). A section of a tetragon with the same area is also shown. The transformation of the dimensions is the same as in Eqs (16).

$$L_1 = c + 2U,\ d = c - 2U = L_1 - 4U,\ V = L_2/4,\quad T = \sqrt{4\,U^2 + 4\,V^2} \tag{16}$$

The volume of a single crystallite is $V_P^S = L_2\,L_3 c$. Using the same approach as the TO geometry, the interface volume, which is related to one crystallite can be calculated via

https://doi.org/10.1017/S0885715614000761 Published online by Cambridge University Press

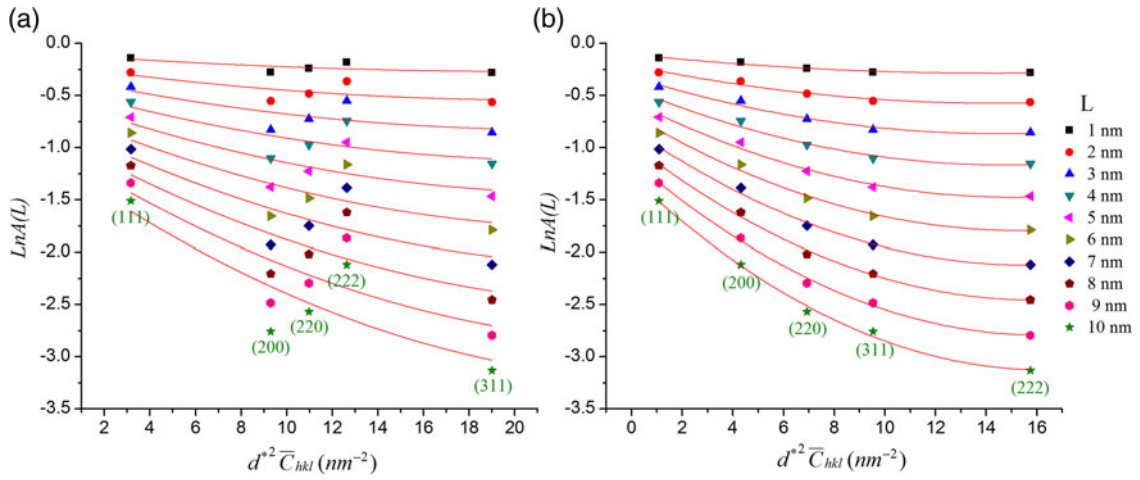

Figure 4. (Color online) The variations of ln$A(L)$ versus $d^{*2}\overline{C}_{hkl}$for (a) edge dislocation character, (b) screw dislocation character, related to sample Cu48 for L = 1 nm to L = 10 nm.

Eq. (17):

$$V_P^{IS} = 2TmL_3 + dmL_3 + \frac{\sqrt{3}}{2}m^2 L_3 + cmL_2 + m^2 d + 2m^2 T + \frac{\sqrt{3}}{2}m^3 \quad (17)$$

Afterward, the number of crystallites and the volume of interface can be calculated via Eqs (18) and (19), respectively:

$$n_P = \frac{V^m}{V_P^S + V_P^{IS}} \quad (18)$$

$$V_{TO}^I = (n_P) \times \left(2TmL_3 + dmL_3 + \frac{\sqrt{3}}{2}m^2 L_3 + cmL_2 + m^2 d + 2m^2 T + \frac{\sqrt{3}}{2}m^3\right) \quad (19)$$

As a matter of fact, the accurate volume fraction of interfaces in each geometry can be derived using the concept of Eq. (20), in which V^S is the volume of one crystallite and V^{IS} is the related interface volume.

$$V^I = 1 - \frac{V^S}{V^S + V^{IS}} \quad (20)$$

A comparison of this approach with the equations of Mütschele and Palumbo is plotted in Figure 8. The crystallite size (D = 6 nm) is considered as the diameter of a sphere and then, equivolume TO and prism are applied. In the case of prismatic geometry, three kinds of crystallites with equiaxed ($L_2 = L_3 = a$), flaky ($L_2 = L_3 = b = 2c$), and columnar ($L_3 = c = 2b$, $L_2 = b$) shapes are modelled. It can be seen that the interface fraction which results from the equation of Mütschele is larger. Moreover, by increasing the boundary thickness, V^I increases linearly and rapidly. Reaching the limit of $3\delta = D$, the interface volume fraction can increase to more than 100% which has no physical meaning. On the other hand, the model of Palumbo exhibits small volume fraction when the interfaces are rather thin; but also shows a high tendency to increase with the increase of boundary thickness. However, it will rise from 100% when the crystallite size is larger than boundary thickness. The interface volume fraction which results from the approach of this study exhibits a slower increase and would not rise from 100% in any situation.

TABLE IV. Contrast factors and the parameter LambdaΛ for the diffraction planes of Fe.

Diffraction plane	$\overline{C}_{edge}$	$\overline{C}_{screw}$	$\overline{C}$	Λ
110	0.1378	0.0470	0.1442	1.3612
200	0.3048	0.3124	0.2699	5.0869
211	0.1795	0.1133	0.1414	4.0833

B. The stored energy of defects

The stored energy can be divided into the interfacial energy and strain energy of dislocations. The GB energies (γ) of Cu and Fe at room temperature are reported to be 716 and

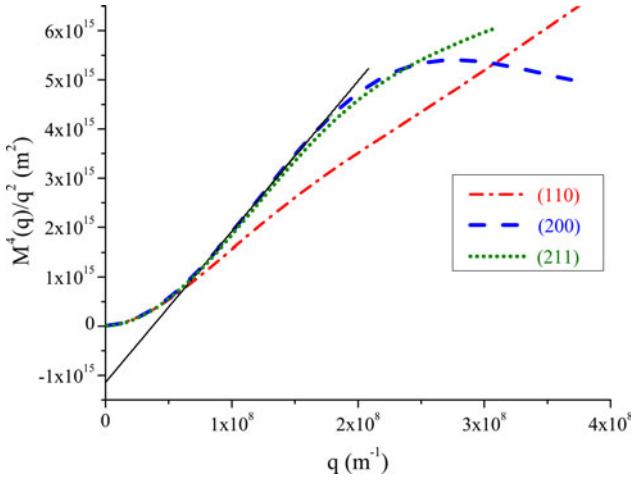

Figure 5. (Color online) The plot of $M_4(q)/q^2$ versus q for the three diffraction peaks of Fe48. The fitted line to the first linear part of (200) curve is shown as an example.

https://doi.org/10.1017/S0885715614000761 Published online by Cambridge University Press

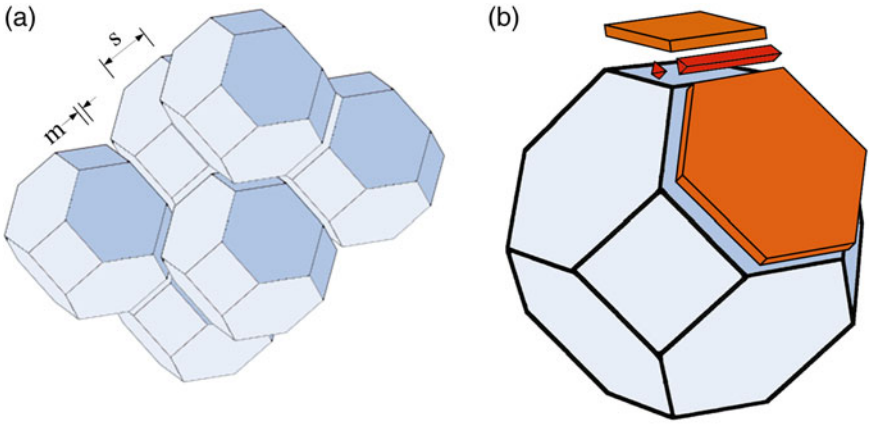

Figure 6. (Color online) (a) Schematic illustration of TO crystallites with a boundary thickness of m at the hexagonal sides, (b) four kinds of interfacial spaces.

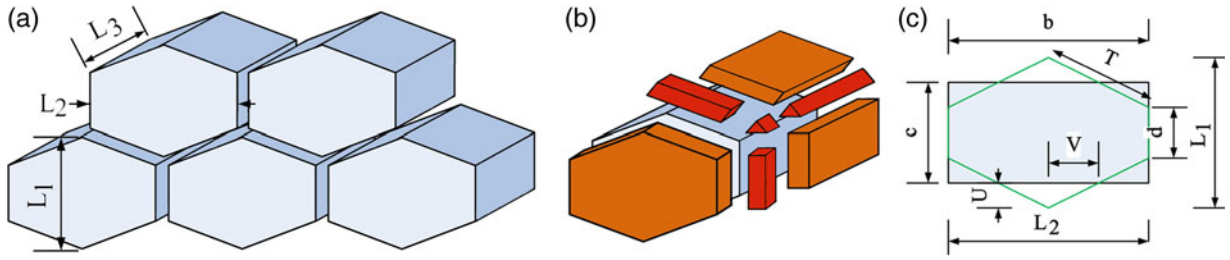

Figure 7. (Color online) (a) Schematic illustration of crystallites as prism with hexagonal base, (b) the seven shapes of boundary volumes which exist in this geometry, and (c) the applied dimensions.

826 mJ m^{-2}, respectively (Zhao, 2006). Assuming $m = 0.5$ nm for relaxed boundaries, the room temperature GB energies of Cu and Fe can be calculated as 1432×10^6 and 1652×10^6 J m^{-3}, respectively. Now the increase of interface width in non-equilibrium boundaries, will result in higher interface volume and more stored energy.

The calculated interface stored energies of the milled powders are shown in Table VI. The crystallite sizes which are resulted from the MWH method (in case of Cu) and the Variance method (in case of Fe) are used as the finest approximations. For all of the prismatic shapes, U is assumed as $0.25c$. Moreover, the average interface thickness in the nanocrystalline milled powders is assumed as 0.8 nm.

The dislocation energy for one mole of material can be calculated via Eq. (21), in which E_D is the dislocation energy for unit length of dislocation line. E_D can be calculated via Eq. (22) (Hull and Bacon, 2001), in which G is the shear modulus, R_e and r_o are the outer and inner radiuses of the dislocation strain field and α is equal to $1/4\pi$ for screw and $1/4\pi\,(1-\upsilon)$ for edge dislocations. υ is the Poisson's ratio.

$$E_{\text{dis}} = \rho E_D V^m \tag{21}$$

$$E_D = \alpha G b^2 \ln\left(R_e/r_0\right) \tag{22}$$

TABLE V. Comparison of the literature data about GB width of metals with various grain sizes and preparation methods.

Metal	Width (nm)	Grain size	Sample preparation	Calculation method	Reference
Ag	0.5	200 μm	Annealing	GB self-diffusion	Sommer and Herzig (1992)
Au	0.6–2.2	A bicrystalline systems	Vapour deposition	An electron diffraction technique	Hagege *et al.* (1982)
	0.8–3.7		Hot-pressing + annealing		
Cu	0.5	50–80 μm	Annealing	GB self-diffusion	Surholt and Herzig (1997)
Cu*	0.8	6.09–12.17 nm	–	Central-symmetry parameter	Li and Xu (2011)
Cu	2.1	About 100 nm	Severe plastic deformation	Electrical resistivity	Islamgaliev *et al.* (1997)
α-Fe	0.5	2.5 mm	Annealing	GB self-diffusion	Inoue *et al.* (2007)
Ni	0.6	500 μm	Annealing	GB self-diffusion	Prokoshkina *et al.* (2013)
Ni*	0.7	5.2–12 nm	–	Geometrical modelling	Caro and Van Swygenhoven (2001)
Ni	3.7	About 100 nm	Severe plastic deformation	Electrical resistivity	Islamgaliev *et al.* (1997)
Pd	0.7–1.1	8–11 nm	Gas condensation + compaction	GB diffusion	Mütschele and Kirchheim (1987)
Pd	>0.6	8.9 nm	Gas condensation + compaction	HRTEM	Wunderlich *et al.* (1990)
Pd	0.4 ± 0.2	5 nm	Gas condensation + compaction	HRTEM	Thomas *et al.* (1990)
α-Ti	0.5	200–300 nm	Equal channel angular pressing	GB diffusion	Fiebig *et al.* (2011)

*The boundary width is result of computer simulation.

https://doi.org/10.1017/S0885715614000761 Published online by Cambridge University Press

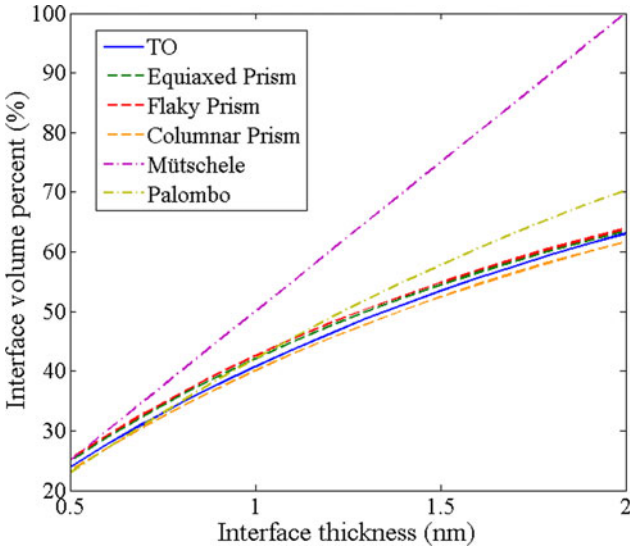

Figure 8. (Color online) Comparison of the GB volume fraction predicted by the equations of Mütschele and Palumbo and the geometrical models of this study. The crystallite diameter is assumed 6 nm and the equivolume shapes are used.

Here, the internal radius is assumed to be equal to the Burgers vector and the external radius is assumed as half of the minimum distance between two dislocations. It is stated that the least distance between two edge dislocations can be calculated via Eq. (23) (Nieh and Wadsworth, 1991), where h is hardness:

$$L_{\min} = \frac{3Gb}{\pi(1-\upsilon)h} \tag{23}$$

Using the material parameters in Table VII, the minimum distance between dislocations in Cu and Fe is calculated to be equal to 5.6 and 4.2 nm, respectively. On the other hand, the dislocation densities form the MWA method (in case of Cu) and the Variance method (in case of Fe) are applied.

As can be seen in Table VI, the main element in the stored energy is the proportion of interfaces. This result is in agreement with the works of Oleszak (Oleszak and Shingu, 1996) and Zhao *et al.* (Zhao *et al.*, 2001; Zhao *et al.*, 2002) on the ball-milled metals. Usage of various crystallite shapes changed the calculated interface energy about 10%. However, the main geometrical parameter, which affects the stored energy is the thickness of interface. For example, increase of m from 0.5 to 1.5 nm results in growth of the interface energy of Cu48 from 626 to 1733 J mol^{-1}.

C. Estimation of the interface width of Cu

The crystallite size of milled Fe is drastically smaller than Cu. Therefore, the calculated stored energy in nanocrystalline Fe is superior. It may be concluded that the released energy during DSC annealing of Fe powder should be higher than Cu. But as can be seen in Table VI, ΔH_{DSC} shows a reverse trend. On the other hand, the crystallite sizes of Cu48 and Cu48-9 are nearly the same, but the released energy of the sample Cu48 is about five times higher than that of Cu48-9.

The DSC curves of samples Cu48 and Cu48-9 can be seen in Figure 9. In the newly milled Cu sample, energy is released between 150 and 340°C via two connected broad peaks, while the first peak is disappeared in the aged powder. It can be concluded that the first exothermic peak was because of the recovery of far from equilibrium boundaries and this recovery was conducted during room temperature ageing. Fecht *et al.* (1990) claimed that the boundary energy of ball milled metals is larger than the energy of fully equilibrated GBs. Here, the difference between the released energy of samples Cu48 and Cu48-9 is 891 J mol^{-1}, which can be considers as excess interface enthalpy. Therefore, this energy should be added to the calculated energies of Table VI. The increased interfacial enthalpy can be seen in Table VIII.

Using the presented geometrical model, the increased GB energy (γ^*) of the milled powder can be calculated indirectly. As an example, the stored interface energy of sample Cu48 in TO geometry is calculated as 1868 J mol^{-1}. Using an assumed boundary thickness of 0.8 nm, γ^* of milled Cu can be calculated as 1369 mJ m^{-2}. As can be seen in Table VIII, the GB energy increased about 1.9 times during mechanical milling. Assuming the GB energy of Cu as 613 mJ m^{-2}, the proportion of γ^* / γ for Cu after 15% deformation and recrystallization at 600°C is measured to be about 1.6 (Grabski and Korski, 1970). This is slightly smaller than the result of this study, which was predictable because the milled powder is not submitted to any thermal process.

On the other hand, the variation of energy in a constant crystallite size can be due to the difference in the thickness of GB. In this way, the thickness of the developed interface region of MM Cu is calculated about 1.6 nm (Table VIII). Further relaxation is possible in longer ageing times. Therefore these amounts should be considered as a minimum quantity for the energy and the thickness of the far from equilibrium boundaries of the ball-milled Cu.

V. CONCLUSION

The crystallite size and dislocation density of the Cu and Fe powders were determined via conventional and

TABLE VI. The calculated dislocation and interface energy of nanostructured Cu and Fe powders in various geometries, besides the released energy during DSC.

	E_{dis} (J mol^{-1})	ΔH^I_{TO} (J mol^{-1})	ΔH^I_P (J mol^{-1})			ΔH_{DSC}(J mol^{-1})
			Equiaxed	Flaky	Columnar	
Cu48	9.6	977	1031	1047	948	1099
Cu48-9	9.5	1056	1027	1043	941	208
Fe48	50.2	5781	5664	5711	5356	948 & 967

https://doi.org/10.1017/S0885715614000761 Published online by Cambridge University Press

TABLE VII. The applied physical properties of Cu and Fe (Zhao *et al.*, 2001; Zhao *et al.*, 2002; Mohamed, 2003).

	Cu	Fe
$V^m \times 10^{-6}$ (m^3 mol^{-1})	7.11	7.09
G (GPa)	46.8	80.7
υ	0.364	0.291
b (nm)	0.2556	0.2482
h (GPa)	3.28	6.45

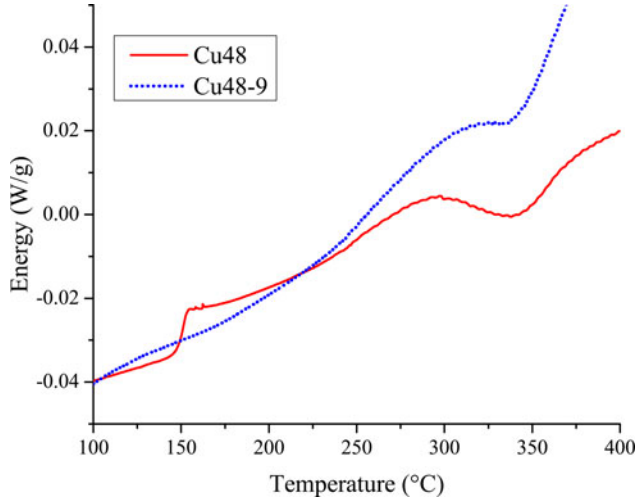

Figure 9. (Color online) The DSC scans for copper powder after 48 h of milling (Cu48) and subsequent room temperature ageing for 9 months (Cu48-9).

TABLE VIII. The total stored interface energy and the calculated energy and thickness of interface, in case of MM copper.

	TO	Prism		
		Equiaxed	Flaky	Columnar
Interfacial enthalpy (J mol^{-1})	1868	1922	1938	1839
γ^* (mJ m^{-2})	1369	1355	1322	1399
γ^* / γ	1.91	1.89	1.85	1.95
Interface thickness (nm)	1.63	1.62	1.57	1.67

advanced XRD analysis methods. The results of WH, MWH, WA, and MWA methods are compared in the case of nanocrystalline Cu powder. The density of dislocations is also calculated via method of WS, besides the modified WA approach. It is clarified that the main dislocation type in the MM Cu powder is screw. In case of nanocrystalline Fe powder, the results of WH, WA, and WS methods are compared to the Variance method.

On the other hand, a geometrical approach is offered for calculation of the inter-crystalline volume using the obtained crystallite sizes. Crystallites with equiaxed, flaky, and columnar shapes are considered. The interface volume fraction is calculated via the expression $1 - V^S/(V^S + V^{IS})$, in which V^S is the volume of each crystallite and V^{IS} the connected interface volume. The specified equations were stated for TO and prism with the hexagonal base. The assumption of various crystallite shapes changed the calculated stored energy almost 10%, while the main geometrical parameter was the GB thickness. The thickness is studied by application of differential scanning calorimetry on room temperature aged Cu powder. It is calculated that the thickness of GB is about 1.6 nm, whereas the interface energy is increased 1.9 times than equilibrium amount.

ACKNOWLEDGEMENT

The corresponding author thanks Dr. Amin Jafari Ramiani for his invaluable help during this research.

Aguilar, C., Martínez, V., Navea, L., Pavez, O., and Santander, M. (**2009**). "Thermodynamic analysis of the change of solid solubility in a binary system processed by mechanical alloying," J. Alloys Compd. **471**, 336–340.

Aste, T., Boose, D., and Rivier, N. (**1996**). "From one cell to the whole froth: a dynamical map," Phys. Rev. E **53**, 6181.

Borbely, A. and Groma, I. (**2001**). "Variance method for the evaluation of particle size and dislocation density from x-ray Bragg peaks," Appl. Phys. Lett. **79**, 1772–1774.

Borbély, A. and Ungar, T. (**2012**). "X-ray line profiles analysis of plastically deformed metals," C. R. Phys. **13**, 293–306.

Borbély, A., Dragomir-Cernatescu, J. Ribarik, G., and Ungar, T. (**2003**). "Computer program ANIZC for the calculation of diffraction contrast factors of dislocations in elastically anisotropic cubic, hexagonal and trigonal crystals," J. Appl. Crystallogr. **36**(1), 160–162.

Boytsov, O., Ustinov, A. I., Gaffet, E., and Bernard, F. (**2007**). "Correlation between milling parameters and microstructure characteristics of nanocrystalline copper powder prepared via a high energy planetary ball mill," J. Alloys Compd. **432**, 103–110.

Caglioti, G., Paoletti, A., and Ricci, F. P. (**1958**). "Choice of collimators for a crystal spectrometer for neutron diffraction," Nucl. Instrum. **3**, 223–228.

Caro, A. and Van Swygenhoven, H. (**2001**). "Grain boundary and triple junction enthalpies in nanocrystalline metals," Phys. Rev. B **63**, 134101.

Delshad Chermahini, M., Zandrahimi, M., Shokrollahi, H., and Sharafi, S. (**2009**). "The effect of milling time and composition on microstructural and magnetic properties of nanostructured Fe–Co alloys," J. Alloys Compd. **477**(1–2), 45–50.

Dong, Y. H. and Scardi, P. (**2000**). "MarqX: a new program for whole-powder-pattern fitting," J. Appl. Crystallogr. **33**(1), 184–189.

Fais, A. and Scardi, P. (**2008**). "Capacitor discharge sintering of nanocrystalline copper," Z. Kristallogr. Suppl. **27**, 37–44.

Fecht, H. J., Hellstern, E., Fu, Z., and Johnson, W. L. (**1990**). "Nanocrystalline metals prepared by high-energy ball milling," Metall. Trans. A **21**, 2333–2337.

Fiebig, J., Divinski, S., Rosner, H., Estrin, Y., and Wilde, G. (**2011**). "Diffusion of Ag and Co in ultrafine-grained a-Ti deformed by equal channel angular pressing," J. Appl. Phys. **110**, 083514–083518.

Grabski, M. W. and Korski, R. (**1970**). "Grain boundaries as sinks for dislocations," Phil. Mag. **22**, 707–715.

Groma, I. (**1998**). "X-ray line broadening due to an inhomogeneous dislocation distribution," Phys. Rev. B **57**, 7535–7542.

Gubicza, J. and Ungar, T. (**2007**). "Characterization of defect structures in nanocrystalline materials by X-ray line profile analysis," Z. Kristallogr. **222**, 567–579.

Guittoum, A., Layadi, A., Tafat, H., and Souami, N. (**2010**). "Structural, microstructural and hyperfine properties of nanocrystalline iron particles," J. Magn. Magn. Mater. **322**, 566–571.

Guo, Y.-B., Xu, T., and Li, M. (**2013**). "Generalized type III internal stress from interfaces, triple junctions and other microstructural components in nanocrystalline materials," Acta Mater. **61**, 4974–4983.

Hagege, S., Carter, C. B., Cosandey, F., and Sass, S. L. (**1982**). "The variation of grain boundary structural width with misorientation angle and boundary plane," Phil. Mag. A **45**, 723–740.

Hull, D. and Bacon, D. J. (**2001**). *Introduction to dislocation* (Pergamon Press), 4th ed.

Inoue, A., Nitta, H., and Iijima, Y. (**2007**). "Grain boundary self-diffusion in high purity iron," Acta Mater. **55**, 5910–5916.

https://doi.org/10.1017/S0885715614000761 Published online by Cambridge University Press

Islamgaliev, R. K., Pekala, K., Pekala, M., and Valiev, R. Z. (**1997**). "The determination of the grain boundary width of ultrafine grained copper and nickel from electrical resistivity measurements," Phys. Status Solidi A **162**, 559–566.

Jang, D. and Atzmon, M. (**2006**). "Grain-boundary relaxation and its effect on plasticity in nanocrystalline Fe," J. Appl. Phys. **99**, 083504–083507.

Khitouni, M., Daly, R., Mhadhbi, M., and Kolsi, A. (**2009**). "Structural evolution in nanocrystalline Cu obtained by high-energy mechanical milling: phases formation of copper oxides," J. Alloys Compd. **475**, 581–586.

Krivoglaz, M. A. (Eds.) (**1996**). *X-ray and Neutron Diffraction in Nonideal Crystals* (Springer, Berlin).

Krivoglaz, M. A. and Ryaboshapka, K. P. (**1963**). "Theory of X-ray scattering by crystals containing dislocations," Phys. Met. Metall. **15**, 18–31.

Langford, J. I. and Wilson, A. J. C. (**1978**). "Scherrer after sixty years: a survey and some new results in the determination of crystallite size," J. Appl. Crystallogr. **11**, 102–113.

Le Burn, P., Gaffet, E., Froyen, L., and Delaey, L. (**1992**). "Structure and properties of Cu, Ni and Fe powders milled in a planetary ball mill," Scr. Metall. Mater. **26**, 1743–1748.

Li, D. X., Ping, D. H., Huang, J. Y., Yu, Y. D., and Ye, H. Q. (**2000**). "Microstructure and composition analysis of nanostructured materials using HREM and FEG-TEM," Micron **31**, 581–586.

Li, M. and Xu, T. (**2011**). "Topological and atomic scale characterization of grain boundary networks in polycrystalline and nanocrystalline materials," Progr. Mater. Sci. **56**, 864–899.

Mitra, G. B. and Mukherjee, P. S. (**1981**). "Application of the method of moments to X-ray diffraction line profiles from paracrystals: native cellulose fibres," J. Appl. Crystall. **14**(6), 421–431.

Mohamed, F. A. (**2003**). "A dislocation model for the minimum grain size obtainable by milling," Acta Mater. **51**, 4107–4119.

Mojtahedi, M., Goodarzi, M., Aboutalebi, M. R., Ghaffari, M., and Soleimanian, V. (**2013**). "Investigation on the formation of Cu–Fe nano crystalline super-saturated solid solution developed by mechanical alloying," J. Alloys Compd. **550**(0), 380–388.

Mula, S., Bahmanpour, H., Mal, S., Kang, P. C., Atwater, M., Jian, W., Scattergood, R. O., and Koch, C. C. (**2012**). "Thermodynamic feasibility of solid solubility extension of Nb in Cu and their thermal stability," Mater. Sci. Eng. A **539**, 330–336.

Mütschele, T. and Kirchheim, R. (**1987**). "Hydrogen as a probe for the average thickness of a grain boundary," Scr. Metall. **21**, 1101–1104.

Nieh, T. G. and Wadsworth, J. (**1991**). "Hall-petch relation in nanocrystalline solids," Scr. Metall. Mater. **25**, 955–958.

Oleszak, D. and Shingu, P. H. (**1996**). "Nanocrystalline metals prepared by low energy ball milling," J. Appl. Phys. **79**, 2975–2980.

Palumbo, G., Thorpe, S. J., and Aust, K. T. (**1990**). "On the contribution of triple junctions to the structure and properties of nanocrystalline materials," Scr. Metall. Mater. **24**, 1347–1350.

Pari Jr, L. D. and Misiolek, W. Z. (**2008**). "Theoretical predictions and experimental verification of surface grain structure evolution for AA6061 during hot rolling," Acta Mater. **56**, 6174–6185.

Prokoshkina, D., Esin, V. A., Wilde, G., and Divinski, S. V. (**2013**). "Grain boundary width, energy and self-diffusion in nickel: effect of material purity," Acta Mater. **61**, 5188–5197.

Sheibani, S., Heshmati-Manesh, S., and Ataie, A. (**2010**). "Structural investigation on nano-crystalline Cu-Cr supersaturated solid solution prepared by mechanical alloying," J. Alloys Compd. **495**, 59–62.

Shimokawa, T., Nakatani, A., and Kitagawa, H. (**2005**). "Grain-size dependence of the relationship between intergranular and intragranular deformation of nanocrystalline Al by molecular dynamics simulations," Phys. Rev. B **71**, 224110–224118.

Sommer, J. and Herzig, C. (**1992**). "Direct determination of grain boundary and dislocation self diffusion coefficients in silver from experiments in typeC kinetics," J. Appl. Phys. **72**, 2758–2766.

Surholt, T. and Herzig, C. (**1997**). "Grain boundary self-and solute diffusion and segregation in general large angle grain boundaries in copper," Defect Diffus. Forum, Trans. Tech. Publ. **143**, 1391–1396.

Suryanarayana, C. (Eds.) (**2004**). *Mechanical Alloying and Milling* (Marcel Dekker, New York).

Thomas, G., Siegel, R. W., and Eastman, J. A. (**1990**). "Grain boundaries in nanophase palladium: high resolution electron microscopy and image simulation," Scr. Metall. Mater. **24**, 201–206.

Tian, H. H. and Atzmon, M. (**1999**). "Comparison of X-ray analysis methods used to determine the grain size and strain in nanocrystalline materials," Phil. Mag. A **79**, 1769–1786.

Ungar, T. and Borbely, A. (**1996**). "The effect of dislocation contrast on X-ray line broadening: a new approach to line profile analysis," Appl. Phys. Lett. **69**, 3173–3175.

Ungar, T., Ott, S., Sanders, P. G., Borbély, A., and Weertman, J. R. (**1998a**). "Dislocations, grain size and planar faults in nanostructured copper determined by high resolution X-ray diffraction and a new procedure of peak profile analysis," Acta Mater. **46**, 3693–3699.

Ungar, T., Révész, Á., and Borbély, A. (**1998b**). "Dislocations and grain size in electrodeposited nanocrystalline Ni determined by the modified Williamson–Hall and Warren-Averbach procedures," J. Appl. Crystallogr. **31**, 554–558.

Warren, B. E. and Averbach, B. L. (**1950**). "The effect of cold-work distortion on x-ray patterns," J. Appl. Phys. **21**, 595–599.

Wilkens, M. (**1976**). "Broadening of X-ray diffraction lines of crystals containing dislocation distributions," Kristall. Tech. **11**, 1159–1169.

Williamson, G. K. and Hall, W. H. (**1953**). "X-ray line broadening from filed aluminium and wolfram," Acta Metall. **1**(1), 22–31.

Williamson, G. K. and Smallman, R. E. (**1956**). "Dislocation densities in some annealed and cold-worked metals from measurements on the X-ray Debye–Scherrer spectrum," Phil. Mag. **1**, 34–46.

Wilson, A. J. C. (**1962**). "On variance as a measure of line broadening in diffractometry general theory and small particle size," Proc. Phys. Soc. **80**, 286.

Wunderlich, W., Ishida, Y., and Maurer, R. (**1990**). "HREM-studies of the microstructure of nanocrystalline palladium," Scr. Metall. Mater. **24**, 403–408.

Yamakov, V., Wolf, D., Phillpot, S. R., and Gleiter, H. (**2002**). "Deformation twinning in nanocrystalline Al by molecular-dynamics simulation," Acta Mater. **50**, 5005–5020.

Zhao, Y. H. (**2006**). "Thermodynamic model for solid-state amorphization of pure elements by mechanical-milling," J. Non-Cryst. Solids **352**, 5578–5585.

Zhao, Y. H., Sheng, H. W., and Lu, K. (**2001**). "Microstructure evolution and thermal properties in nanocrystalline Fe during mechanical attrition," Acta Mater. **49**, 365–375.

Zhao, Y. H., Lu, K., and Zhang, K. (**2002**). "Microstructure evolution and thermal properties in nanocrystalline Cu during mechanical attrition," Phys. Rev. B **66**, 854041–854048.

https://doi.org/10.1017/S0885715614000761 Published online by Cambridge University Press